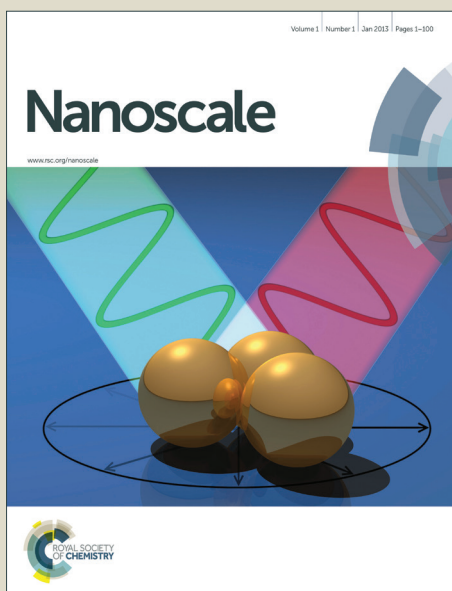


# Nanoscale

Accepted Manuscript



This is an *Accepted Manuscript*, which has been through the Royal Society of Chemistry peer review process and has been accepted for publication.

*Accepted Manuscripts* are published online shortly after acceptance, before technical editing, formatting and proof reading. Using this free service, authors can make their results available to the community, in citable form, before we publish the edited article. We will replace this *Accepted Manuscript* with the edited and formatted *Advance Article* as soon as it is available.

You can find more information about *Accepted Manuscripts* in the [Information for Authors](#).

Please note that technical editing may introduce minor changes to the text and/or graphics, which may alter content. The journal's standard [Terms & Conditions](#) and the [Ethical guidelines](#) still apply. In no event shall the Royal Society of Chemistry be held responsible for any errors or omissions in this *Accepted Manuscript* or any consequences arising from the use of any information it contains.

Cite this: DOI: 10.1039/c0xx00000x

www.rsc.org/xxxxxx

ARTICLE TYPE

## Functionalization of graphene oxide nanostructures improves photoluminescence and facilitates their use as optical probes in preclinical imaging

Neeraj Prabhakar,<sup>abc</sup> Tuomas Näreoja,<sup>\*b</sup> Eva von Haartman,<sup>ac</sup> Didem Şen Karaman,<sup>ac</sup> Sergey A. Burikov,<sup>d</sup> Tatiana A. Dolenko,<sup>d</sup> Takahiro Deguchi,<sup>b</sup> Veronika Mamaeva,<sup>e</sup> Pekka E. Hänninen,<sup>b</sup> Igor I. Vlasov,<sup>fg</sup> Olga A. Shenderova<sup>h</sup> and Jessica M. Rosenholm<sup>\*ac</sup>

Received (in XXX, XXX) XthXXXXXXXXXX 20XX, Accepted Xth XXXXXXXXXXXX 20XX

DOI: 10.1039/b000000x

Recently reported photoluminescent nanographene oxides (nGO), i.e. nanographene oxidised with sulfuric to nitric acid mixture (SNOx method), have tuneable photoluminescence and are scalable, simple and fast to produce optical probes. This material belongs to the vast class of photoluminescent carbon nanostructures, including carbon dots, nanodiamonds (ND), graphene quantum dots (GQD), which all demonstrate a variety of properties that are attractive for biomedical imaging such as low toxicity and stable photoluminescence. In this study, the nGOs were organically surface-modified with poly(ethylene glycol) – poly(ethylene imine) (PEG-PEI) copolymers tagged with folic acid as affinity ligand for cancer cells expressing folate receptors. The functionalization enhanced both their cellular uptake and quantum efficiency of the photoluminescence as compared to non-modified nGOs. The nGOs exhibited an excitation dependent photoluminescence that facilitated their detection with a wide range of microscope configurations. The functionalized nGOs were non-toxic, they were retained in the stained cell population over a period of 8 days and they distributed equally between daughter cells. We have evaluated their applicability in *in vitro* and *in vivo* (chicken embryo CAM) models to visualize and track migratory cancer cells. The good biocompatibility and easy detection of the functionalized nGOs suggest that they could address the limitations faced with quantum dots and organic fluorophores in long-term *in vivo* biomedical imaging.

### Introduction

Carbon nanostructures have emerged as a novel family of nanomaterials with biomedical prospects<sup>1,2,3</sup> especially so due to their unique optical properties that have ascribed them with potential to replace currently used nanostructured imaging probes such as quantum dots (QDs)<sup>4,5</sup>. Composed of the major element of life, carbon, these materials are thus associated with lower toxicity than their heavy metal-composed semiconductor counterparts<sup>6</sup>. There are several categories of carbon-based luminescent nanoparticles, such as soot, activated carbons, graphite, carbohydrates<sup>7,8</sup> nanotubes, and nanodiamonds<sup>9</sup> that have been used as precursors to luminescent carbon-based nanomaterials using oxidizing conditions at elevated temperatures. Nano-graphene oxide nanoparticles are a group of fluorescent carbon-based structures that is related to graphene oxide (GO). The atomic structure of GO is comprised of a graphene basal plane with a non-uniform coverage of oxygen-containing functional groups, such as epoxy and hydroxyl groups, resulting in  $sp^2$  carbon islands of a few nanometers in size isolated within a defective  $sp^3$  carbon network<sup>10</sup>. Edges of the GO can contain other various oxygen-containing groups<sup>7,9</sup>. Typical C:O ratios in GO range between 2 and 4. While

luminescent GO structures can be relatively large, isolated structures of nanometer size can also be produced (nGO)<sup>11,12</sup>. A popular method of the production of photoluminescent GO-based structures is the creation of nanosized  $sp^2$  islands by a partial reduction of graphite oxide. The latter is typically obtained by oxidizing graphite under harsh conditions, followed by exfoliation into predominantly single-layer sheets. The fluorescence of GO-based structures has been reported from the visible to the NIR range, and the maximum intensity is located between 500 and 800 nm<sup>13,14</sup>. Photoluminescence in GO-based structures was proposed to originate from emissive electronic transitions within a band gap formed by quantum confinement in the isolated  $sp^2$  carbon islands, as well as by functionalized surface defect sites<sup>13,14</sup>. While nGO particles demonstrate bright stable luminescence, photoluminescent (PL) nanocarbons obtained by different chemical treatments vary widely in structure and composition as well as their PL properties. In this study, we have used nano-graphite/graphene oxide (nGO) synthesized by oxidizing micro- and/or nanographite in a 3:1 sulfuric to nitric acid mixture (SNOx). Recently, we demonstrated that the SNOx method can be used to produce PL

carbon nanostructures by oxidation of micrographite, nanographite and other graphitic source materials at temperatures exceeding 100°C<sup>15,16</sup>. This acid mixture functions as an exceptional graphite intercalation compound which facilitates cleavage and oxidation that initially form graphite oxide followed by graphene oxide produced by exfoliation. It was possible to tune the PL emission of the reaction suspension from the blue to red by tuning the combination of reaction temperature and time. Peng *et al.* showed that this mixture can oxidize carbon fibers<sup>17</sup> and that increasing the reaction temperature causes a blue-shift of the PL emission wavelength. The advantages of using the SNOx method for production of nGO include scalability, simplicity and fast production time<sup>16</sup>.

Here, the use of photoluminescent nGO produced by the SNOx method in biomedical imaging was demonstrated both *in vivo* and *in vitro* as well as was spectrophotometrically evaluated for its excitation wavelength-dependent photoluminescent nature. To further expand the applicability of the inorganic nGO, they were organically modified in order to 1) increase the colloidal stability in the complex physiological environment, 2) promote the cellular uptake by adding functional coatings interacting with the cell membrane, and 3) enhance the specific affinity towards cancer cells by surface-anchoring of targeting ligands<sup>18</sup>. We utilized folic acid (FA) as the affinity ligand, which was covalently coupled to the poly(ethylene imine) – poly(ethylene glycol) copolymer<sup>19</sup> and subsequently coated onto the nGO through electrostatic adsorption. We have also evaluated their potential as an *in vitro* label for cell staining and utilized their excitation dependent emission for detection.

To evaluate the potential of nGO for labelling and subsequent detection of labelled tumor cells in an *in vivo* setting, we used the chick embryo chorioallantoic membrane (CAM) model<sup>20,21,22,23</sup>. The CAM model has been put forward as a preferable method to conduct short-term *in vivo* experiments in order to avoid animal trials. The CAM model is inexpensive, easy to analyse with light microscopy, robust, and it is not subject to laboratory animal legislation nor does use of it require specialized facilities. Moreover, it is recommended as an alternate model in the 3R principle (Replacement, Reduction and Refinement of vertebrate laboratory animals) thus replacing costly and time-consuming animal experiments. CAM serves as a source of angiogenic blood vessels that in addition to nurturing developing tumors, provides an organotypic environment for tumor cell intravasation, dissemination, and vascular arrest, but also a repository where arrested cells extravasate to form micro metastatic foci<sup>22,24,25</sup>. Here we show that the studied nano-graphene oxide nanoparticles show considerable potential to become a versatile, safe and long-term probe for live light microscopy utilizing the CAM model.

## 1. Experimental

### 1.1 Particle preparation and characterization

#### 1.1.1 Surface functionalization of nGO particles

nGO was produced by oxidation of ~400 nm natural nanographite (Nanostructured & Amorphous Materials Inc., Houston, TX) in the 3:1 mixture of 95–98% sulphuric acid to 68% nitric acid for 2 hours. The supernatant and residue were

separated by centrifugation. The acidic mixture was evaporated from the supernatant at 350°C and the brownish residue was resuspended in DI water at a concentration of 5 mg/ml. For the synthesis of copolymers, with and without FA, an in-house procedure was applied as follows. The chemicals that were used for copolymer synthesis, poly (ethylene glycol) methyl ether (mPEG, 5,000 molecular weight), polyethyleneimine (PEI, 25,000 molecular weight), hexamethylene diisocyanate (HMDI) (>99%) were supplied by Sigma Aldrich. Folic acid (FA) ligand (>97%) was purchased from Sigma. For the FA-conjugated copolymer preparation, Maleimide-PEG-OH (MW of PEG 5kDa, mal-PEG-OH) polymer from JENKEM Technology was used as a starting reagent. The organic solvents, anhydrous chloroform and diethyl ether, were from Riedel-de Haën and J.T.Baker, respectively. Milli-Q water (18.2 Ω) was used throughout the study. Only analytical grade chemicals were used.

#### 1.1.2 Copolymer synthesis

The synthesis was carried out as follows: first, mPEG reagent was activated by HMDI for further reaction with PEI. For this purpose, 1g of mPEG was dissolved in 25mL of CHCl<sub>3</sub> and 3.2 mL HMDI was added. The reaction was carried out at 60 °C under reflux and with stirring overnight. After the reaction, the activated mPEG polymer was collected by precipitation with the addition of diethyl ether and collected by centrifugation at 5,000 rpm for 10 minutes. After collecting the activated mPEG polymer, it was dried under vacuum. As a second step of copolymer preparation, 0.6 g of activated mPEG was reacted with 0.8 g of 25kDa PEI in 25 mL of CHCl<sub>3</sub> under the same conditions mentioned for activation of mPEG polymer. After the reaction, the obtained product was purified by diethyl ether and vacuum dried. The folic acid – copolymer conjugate was prepared as follows: First, 150 mg of mal-PEG-OH was dissolved in 15 mL of CHCl<sub>3</sub> and 0.482 ml HMDI was added to the reaction solution (1:100 molar ratio of mal-PEG-OH:HMDI). The reaction was carried out overnight at 60°C under reflux with stirring. Then, the activated mal-PEG-HMDI polymer was purified by the addition of diethyl ether and centrifugation (5000 rpm, 10 min). As a second step, 25kDa PEI polymer was reacted with the activated mal-PEG-HMDI with the molar ratio of 6:1 (137 mg of mal-PEG-HMDI dissolved in 15 ml of CHCl<sub>3</sub> and 110 mg of PEI was added to the reaction solution) at 60°C under reflux for overnight. The product (mal-PEG-PEI) was purified and collected as mentioned above. As a third step, cysteamine-conjugated folic acid was prepared in order to react with mal-PEG-PEI. For the cysteamine conjugated folic acid (FA-Cys) preparation, FA was dissolved in DMF and activated with HATU (1-[Bis(dimethylamino)methylene]-1H-1,2,3-triazolo[4,5-b]pyridinium 3-oxid hexafluorophosphate) for 15 min (molar ratio 1:1) and cysteamine was also dissolved in DMF and activated with DIPEA (N,N-Diisopropylethylamine) for 15 min (molar ratio 1:1). The reaction solutions were mixed and kept under stirring for 24h at RT. After the reaction was completed, the FA-Cys was precipitated with (30:70) acetone: diethyl ether mixture, and separated by centrifugation at 10 000 rpm for 10 min and vacuum dried. The obtained yellow powder was kept in the freezer (at -18 C) for further usage. For FA-Cys conjugation to the copolymer, 160 mg of mal-PEG-PEI copolymer was dissolved in 16 ml HEPES buffer and 8.8 mg of FA-Cys was also

dissolved in 8 ml of HEPES buffer and the solutions were mixed and kept under stirring for 3 h at room temperature. Then, the reaction solution was dialyzed against DI water for 24 h and freeze dried. The obtained yellow powder of FA-PEG-PEI copolymer conjugate was kept in the freezer at -18°C for further usage.

### 1.1.3 Copolymer coating

The nGO structures were coated with the in-house synthesized poly(ethylene glycol)-poly(ethylene imine) (mPEG-PEI) copolymers with (Cop-FA) and without (Cop) folic acid (FA). The nGO particles were dispersed in HEPES (25 mM, pH 7.2) using ultrasonication and purified by dialysis for 24 h before surface coating. The solvent was discarded and changed to a fresh one three times during the dialysis. The nGO particles were dispersed in HEPES (25 mM, pH 7.2) using ultrasonication. The copolymers were dissolved to a concentration of 1 mg/mL in HEPES and 10-50 wt-% (with respect to the nGO) was dropwise added to the nGO dispersion during ultrasonication for a final particle concentration of 1 mg/mL to find the optimal amount. The sample was stirred at RT overnight. Copolymer-coated nGO was denoted nGO-Cop.

### 1.2 PL measurements of nGO suspensions

The PL of nGO (1mg/ml in HEPES, pH 7.2) was measured on a PTI Quanta-Master spectrofluorimeter (Photon Technology International, Lawrenceville, NJ). The excitation and the emission slits were set to 5nm. The measurements were performed in quartz cuvettes with a light path length of 1cm. Fluorescence intensity of nGO was detected with excitation wavelengths at 405, 488 and 532 nm.

### 1.3 Quantum yield measurements

Excitation of PL spectra was performed by argon laser (wavelength 488 nm, output power 350 mWt) and diode lasers (wavelengths 405 nm and 532 nm). The system of registration consisted of a monochromator (Acton, grades 900 and 1800 g/mm, focal length 500 nm, spectral resolution 1 cm<sup>-1</sup>) and two detectors (PMT and CCD-camera). PL spectra in the range 410-800 nm were measured by PMT in the mode of step-by-step registration. The measurements were performed in quartz cuvettes with light path length of 1cm. The temperature of the samples during experiment was maintained constant equal to (22.0 ± 0.2)°C in a thermostabilized cuvette. The spectra were normalized to the power of laser radiation and to the spectrum accumulation time.

### 1.4 Cellular internalization, toxicity and microscopy

The cytocompatibility of nGO, nGO-Cop, nGO-Cop-FA nanoparticles was evaluated using WST-1 cell viability assay (Roche Diagnostics). 10,000 HeLa cells per well were grown in a 96 well plate in DMEM (10%FCS, 1% amino acids, 1% penicillin-streptomycin) and incubated overnight to adhere. Then a) pure nGO, b) nGO-Cop, c) nGO-Cop-FA particles were sonicated for 15 min and added to 1ml of pre-warmed (37°C) growth medium at three different 10-fold increasing concentrations of 1 µg, 10 µg, 100 µg. Then, the growth medium containing particles was further sonicated for 15min. The growth media of cells in 96 well plates was replaced with media

containing three different concentrations of a) pure nGO, b) nGO-Cop, c) nGO-Cop-FA. 5 µM of staurosporine (toxin) was added as a positive control, whereas negative control cells were untreated (pure cell media only). After incubating the particles for 48 h at 37°C, 5% CO<sub>2</sub>, 10 µl of WST-1 cell proliferation reagent (Roche Diagnostics, Germany) was added to each well containing 100 µl of cell growth media, and the plate was again allowed to incubate for 3 h at 37°C, 5% CO<sub>2</sub>. After incubation, the absorbance was read at 430 nm by Tecan Ultra microplate reader (MTX Lab Systems, Inc.). The number of viable cells was correlated with the observed absorbance from each individual sample.

### 1.4.1 CAM model preparation of ex ova culture

Fertilized chicken eggs were obtained from LSK Poultry (Turku, Finland). Eggs were placed in a rotary thermostat incubator at 37°C at 65% relative humidity. At day 3, eggs were wiped gently with 70% ethanol with paper towel. Eggshells were carefully cut using a rotating saw without damaging the inner membranes. The egg's entire content was very gently transferred into a sterile weighing boat containing 5 ml of DMEM growth medium (1% penicillin-streptomycin) and grinded egg shell was added to provide calcium. Weighing boats were covered from the top with petri dishes. The weighing boats containing eggs were allowed to incubate till day 8 at 37°C at 65% relative humidity.

### 1.4.2 Preparation of in ova culture

Fertilized chicken eggs were obtained from LSK Poultry (Turku, Finland). Eggs were placed in a rotary thermostat incubator at 37°C at 65% relative humidity. At day 3, eggs were gently wiped with 70% ethanol with paper towel. A small hole was made on the egg shell and then covered with Parafilm®. The eggs were allowed to develop until day 8 at 37°C at 65% relative humidity. Before tumor implantation, the existing holes in the eggs shell were carefully opened to facilitate tumor implantation and subsequent imaging.

### 1.4.3 In vivo multiphoton imaging of implanted tumors

The experimental setup consisted of TCS SP5 MP (Multi-photon, Leica microsystems), LASAF software (Leica application suite), Non-descanned detectors (NDD) and 20X dip objective. Multiphoton microscopy was performed with Ti-sapphire femtosecond pulse (Chameleon Ultra, Coherent Inc, CA, USA) at 800 nm for excitation of nGO-Cop-FA implanted tumors of live CAM membrane placed on pre-warmed gel packs at 37°C. The emission from particles was collected using NDD detectors (NDD1) at 430-480nm.

## Results and discussion

### 2. 1. Particle preparation and characterization

Nano-graphite/graphene oxide was synthesized according to our previously reported procedure by SC Hens *et al.*<sup>16</sup> The prepared nGO was kept in aqueous suspension at a concentration of 5 mg/ml as a stock. To potentially enhance their performance in a biological setting (*in vitro* and *in vivo*) these nGO were also further coated with PEG-PEI copolymers via electrostatic adsorption<sup>19</sup> by titration against copolymer concentration by

dynamic light scattering to find the optimal amount of copolymer to be used (**Table 1**). As a result from the oxidation process, the surface of nGO possesses abundant carboxylic acid (COOH) groups, which renders the nGO surface negatively charged at neutral pH (**Table 1**). Thus, electrostatic adsorption can be readily realized by utilizing the polycation PEI as ‘anchor’ between the nGO surface and neutral PEG chains. When an optimal copolymer ratio had been found, a third nGO sample was prepared using FA-PEG-PEI copolymers, i.e. with FA conjugated to the terminal end of PEG (see **Scheme 1**) to be used as affinity ligands towards cancer cells <sup>26</sup>.

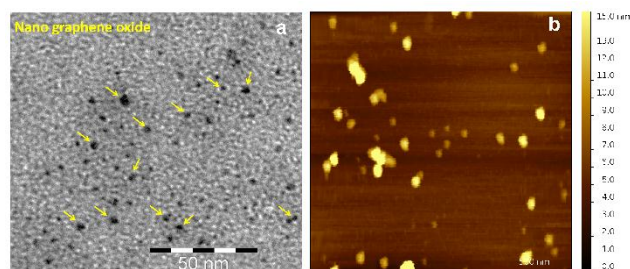
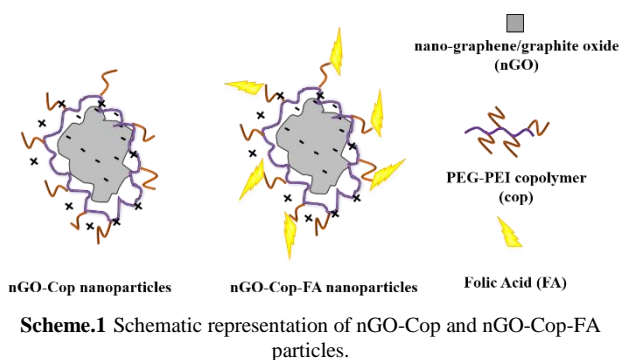


**Figure.1** Size distribution of nGO imaged with a) TEM and b) AFM.

Nevertheless, the DLS measurements were performed in HEPES buffer which suggested that slight nGO aggregation may have occurred; especially for the non-polymer-coated nGO (hydrodynamic diameter > 100 nm). Here, it can be seen for the plain nGO particles that they have a strong natural tendency to aggregate under these conditions. To examine the size of single particles we conducted TEM and AFM imaging, of dried material from the same starting suspension (**Figure 1**). We saw a number of aggregates with uncoated nGO and less with the coated materials. However, we were able to measure the sizes of single particle’s median diameters as: nGO 4.3 nm; COP 9.6 nm; COP-FA 11.1 nm (**Figure S4**). Consequently, apart from other added benefits of surface functionalization, the surface coating also efficiently prevents particle aggregation and provides colloidal stability in aqueous suspensions (**Table 1**).

**Table 1** Hydrodynamic size and zeta potential of pure and surface functionalized nGO.

Sample	Size (number PSD) <sup>a</sup> [nm]	PDI	Zeta <sup>b</sup> [mV]
nGO	112.1 (100%)	0.287	-22.5
nGO-Cop 30 wt-%	36.39 (99.7%)	0.32	13.7
nGO-Cop-FA 30 wt-%	19.08 (100%)	0.34	-5.1

<sup>a</sup> The number size distribution was used for determining the hydrodynamic size of nGO. <sup>b</sup> Both DLS and electrokinetic measurements were carried out in HEPES buffer (25 mM, pH 7.2).

## 2.2. PL properties of nGO

Excitation-dependent emission has been demonstrated by nGO over the entire visible range. GO has shown unique emission properties due to emissive electronic transitions within a band gap formed by quantum confinement in the isolated  $sp^2$  carbon islands. To investigate this, the fluorescence properties of our nGO were characterized by spectrofluorimetry. Many different optical centres were detected, which were dependent on the excitation wavelength (**Figure 2**). A systematic fluorescence spectrophotometric evaluation showed that emission maxima occur at approximately 70-90 nm from the excitation wavelength. PL spectra of water suspensions of nGO, nGO-Cop, and nGO-Cop-FA nanoparticles with the same concentration 0.01 mg/ml under excitation wavelength 405, 488 and 532 nm are presented in **Figure 2a-c**.

This surface coating should further enhance the colloidal stability of nGOs under biological/physiological conditions due to the electrostatic stabilization provided by PEI combined with the steric stabilization provided by PEG <sup>27</sup>. The dispersability of all three resulting nGO samples (pure nGO, nGO-Cop and nGO-Cop-FA) were confirmed with dynamic light scattering (DLS) and the alteration in surface charge upon copolymer coating was followed by electrokinetic measurements ( $\zeta$ -potential) (**Table 1**). Upon copolymer adsorption, the net surface charge at physiological pH converted from negative to positive due to the high positive charge density of PEI, <sup>28</sup> but was still rendered lower than that of characteristic of nanoparticle surfaces functionalized with PEI only due to partial shielding ( $\zeta$ -potential measured at a larger distance from the particle surface) from the PEG chains. Further, the conjugation of FA resulted in lowering of the net surface charge to slightly below zero due to the partial deprotonation of folic acid at physiological pH <sup>29</sup>. The morphology and size of nGO particles (nGO, nGO-Cop and nGO-Cop-FA) were studied by applying low voltage (80kV) transmission electron microscopy (TEM) and atomic force microscopy (AFM). TEM at low magnification revealed the nGO particles were of different sizes (**Figure S3**), but all typically below 10 nm. However, even at high magnification, it was difficult to properly investigate the particle morphology in great detail. The particles can be seen uniformly dispersed over the TEM grid (**Figure 1a**). Therefore, AFM was further applied to study the size distribution. AFM shows a similar size distribution pattern (**Figure 1b**) as observed by TEM. We recorded a wide distribution of sizes typically below 10 nm with some larger aggregates in the nGO sample (**Figure S4**).

Cite this: DOI: 10.1039/c0xx00000x

www.rsc.org/xxxxxx

ARTICLE TYPE

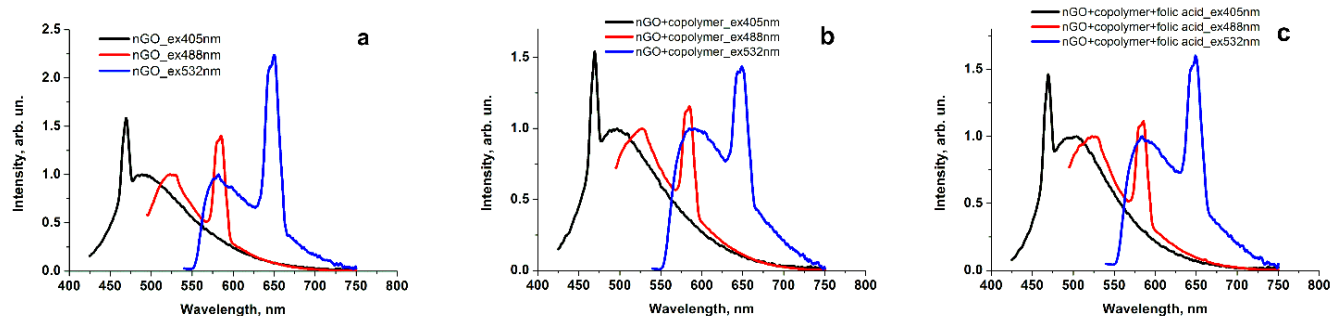


**Figure 2** PL emission spectra of pure graphene oxide nanoparticles (nGO) showed excitation dependent emission peaks. The emission analysis of 1mg/ml nGO was carried out on a PTI Quanta-Master spectrofluorimeter. a) PL spectra of nGO water suspension with concentration 0.01 mg/ml under different excitation wavelengths. b) PL spectra of, nGO-Cop water suspension with concentration 0.01 mg/ml under different excitation wavelengths. c) PL spectra of, nGO-Cop-FA water suspension with concentration 0.01 mg/ml under different excitation wavelengths. All spectras are normalized to the fluorescence maximum.

Comparative analysis of PL spectra of the suspensions of nGO, nGO-Cop, nGO-Cop-FA nanoparticles confirms high and stable PL properties of all three prepared suspensions. PL spectra of the water suspensions with the same concentration 0.01 mg/ml under excitation wavelength 405 nm are presented in **Figure 3**.

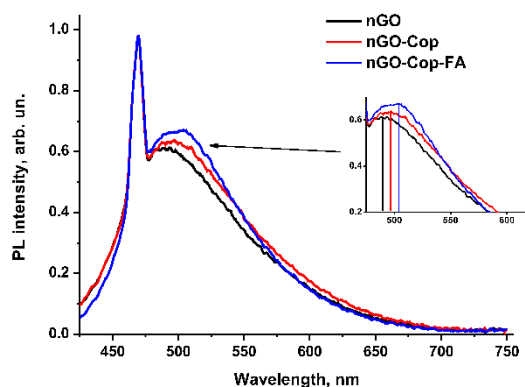


**Figure 3** PL spectra of water suspensions of nGO, nGO-Cop, nGO-Cop-FA nanoparticles with the same concentration 0.01 mg/ml (excitation wavelength 405 nm). Spectra are normalized to maximum of Raman water valence band. The PL maximum in the obtained spectra of water suspensions of nGO, nGO-Cop, nGO-Cop-FA moves to the "red side" by the following way:  $\lambda_{\text{max}}^{\text{PL}}(\text{nGO}) = 489 \text{ nm}$ ,  $\lambda_{\text{max}}^{\text{PL}}(\text{nGO-Cop}) = 497 \text{ nm}$ ,  $\lambda_{\text{max}}^{\text{PL}}(\text{nGO-Cop-FA}) = 504 \text{ nm}$ . The maximum of water Raman valence band (470 nm) does not shift. This band plays role of the inner benchmark for our quantitative estimations of the changes of PL of nanoparticles.

The nanoparticle concentration above was selected so that registration of Raman valence band of water was reliable (which was needed to calculate the  $F_0$  parameter, see below). This band was the internal reference point in the PL measurements. As can be seen from **Figure 3**, coating of nGO with the copolymers (Cop and Cop-FA) does not quench PL but actually slightly increases it. The parameter  $F_0$  was used for a quantitative characterization

of the PL intensities of the samples, which is the ratio of integral intensity of fluorescence to integral intensity of water Raman valence band<sup>30</sup>. Values of  $F_0$  were determined for all the studied suspensions (**Table 2**). The obtained results showed that organic coating of nGO with copolymers slightly increased the PL properties. Furthermore, measurements of nGO PL spectra every day during several months showed very high fluorescence stability. All in all, the observed PL properties render all three (nGO, nGO-Cop, nGO-Cop-FA) nanoparticle formulations very promising for biomedical imaging purposes.

The graphene oxides and similar carbon structures reported in literature has very variable quantum efficiency, which is mainly dependent on the synthesis, functionalization and structure<sup>31</sup>. The latest study by Wei *et al*, demonstrated that the quantum efficiency of graphene oxide is inversely proportional to increase in size. Typically, in the Wei *et al*. study, the quantum efficiencies of different (graphene oxide) particle sizes of 43.5 nm, 23.1 nm and 12.3 nm were 0.83%, 2.63% and 3.73%<sup>31</sup>. Moreover, another study carried by Mei *et al*. has shown that the graphene oxide quantum efficiency can be effected by the  $\text{NH}_2/\text{C}$  ratio using different alkylamine functionalizations<sup>32</sup>. Therefore, in our case, for our nGO produced by a different synthesis route<sup>16</sup> and subject to organic surface coating, it is critical to evaluate them for their PL properties. Thus, to further investigate the unique optical properties of the resultant nGO composites, a PL study was carried out after surface coating them with the organic PEG-PEI copolymers, which is a widely used strategy for organic surface modification of nanomaterials intended for biomedical applications. For inorganic nanoparticles, we have previously shown that this type of coating can promote an enhancement in cellular uptake<sup>19,33</sup>. The present study was intended to observe the effects of organic surface coating on the PL properties of nGO. For water suspensions of all prepared nanoparticles, the quantum yields were measured, and these values are presented in **Table 2**.

**Table 2** Characteristics of PL properties of nGO water suspensions.

Parameters	nGO	nGO-Cop	nGO-Cop-FA
<b>Quantum yield</b>	4.80%	6.20%	7.10%
$F_0$ ( $\lambda_{exc}=405$ nm)/ $\max_{PL}$	15.8 / 493 nm	16.1 / 498 nm	17 / 501 nm
$F_0$ ( $\lambda_{exc}=488$ nm)/ $\max_{PL}$	5.3 / 527 nm	7.7 / 528 nm	8.7 / 528 nm
$F_0$ ( $\lambda_{exc}=532$ nm)/ $\max_{PL}$	3.2 / 588 nm	5.4 / 589 nm	7.6 / 590 nm

Evidently, nGO particles coated by copolymers exhibited better quantum yield values than without organic coating. Consequently, the result demonstrates that organic surface modification is vital not only for proper colloidal stability and presumed cellular applicability, but also for enhancement of the PL properties of nGO. The mechanism of quantum efficiency improvement by organic modification is still not properly understood, which is why more studies are required to fully understand the chemical mechanism of organic polymers in improvement of PL properties.

### 2.3. Cytocompatibility

Cytotoxicity analysis is a prerequisite before any further evaluations involving biological systems. Different concentrations and surface functionalization (in the present case, PEG-PEI copolymers and folic acid) may change the biocompatibility of a material even if it has inherently been reported as “safe”. The biocompatibility of each separate surface modification of graphene oxide nanoparticles with HeLa cancer cells was thus evaluated. Staurosporine, an established kinase inhibitor cellular toxin, was used as positive control for toxicity. WST-1 cell viability assay was used to evaluate the cytocompatibility of all three prepared nGO suspensions at a 10-fold increasing concentration to examine the effects of both higher concentrations coupled with different surface chemistries.

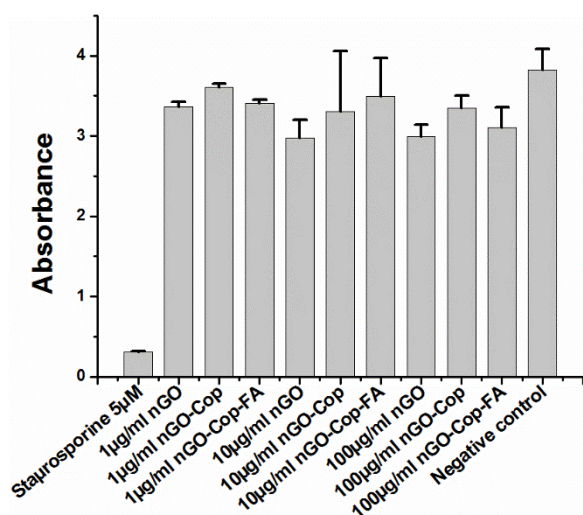


**Figure.4** Graphical representation of cell viability evaluated by WST-1 assay. The absorbance values are directly proportional to the number of viable HeLa cells. Staurosporine (5µM) was added to the HeLa cells as positive control, whereas the negative control HeLa cells were untreated. 10 fold increasing particle concentrations were added of nGO and surface modified nGO nanoparticles.

The cytocompatibility evaluation showed that the pure graphene oxide (nGO) and surface-coated nGO nanoparticles even at higher concentrations are safe for cells under the experimental conditions used. The absorbance values for negative controls (cells without particles) and nGO particle-incubated cells showed equivalent viability for different surface chemical modifications. nGO-incubated cells remained highly viable after 48h incubation in comparison to Staurosporine-treated cells. The cell viability remained high even at concentrations up to 100 µg/ml. Neither upon the addition of copolymers nor at conjugation with folic acid, did we observe any cytotoxicity. Previously, we found that nanocomposites based on PL nanodiamonds coated with similar copolymers were also cytocompatible<sup>33</sup>. The functionalization appeared to provide a small but non-significant increase in tolerability of the nGOs, possibly due to lower tendency to form aggregates (**Figure 4**). With the toxicity levels determined, all nGO variants were established to be safe and applicable for further *in vitro* and *in vivo* applications.

### 2.4. Cellular imaging

The optical detectability of cells labelled with nGO *in vitro* was investigated by confocal and two-photon excitation microscopy. *In vitro* detectability was evaluated for HeLa, MDA-MB-231 and A549 cancer cells incubated with nGO-Cop-FA nanoparticles (**Supplementary Info Figure S6**). These three cell lines were chosen due to their overexpression of folate receptors (FR)<sup>34,35,36</sup>. The surface-functionalized nGO nanoparticles could readily be detected by confocal as well as two-photon imaging (**Figure 5a-b**). The bright photoluminescence from nGO-Cop-FA was detected throughout the cells, which indicated that nGO-Cop-FA particles were efficiently internalized by the different cancer cells; and finally they were localized outside the nucleus (**Figure 5**). The particles seem to be localized in endosomes, where they are collected as a result of their trafficking into these intracellular compartments after cellular uptake by endocytosis,<sup>37</sup> consequently forming intracellular aggregates of detectable size. Smaller nGO clusters can also be seen spread across the entire cytoplasm, which should be a result of endosomal escape of the particles; a process which can be facilitated by the aid of PEI. The cellular uptake enhancement followed by endosomal escape facilitated by surface coating of inorganic nanoparticles with corresponding PEG-PEI copolymers has been reported previously<sup>28,33,38</sup>. Here, the efficient internalization of particles imparted by the surface coating improves the overall detectability of cells, promoting the use of nGO as cellular labels.

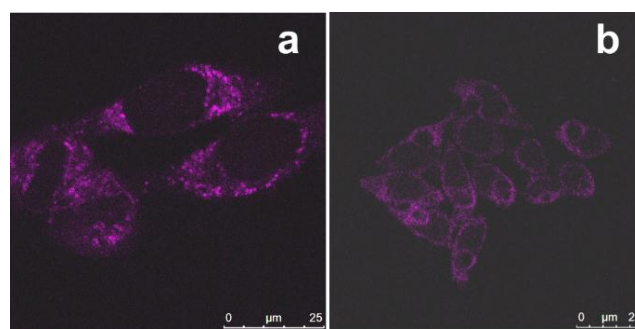


**Figure.5** PL images from fixed HeLa cells incubated with a 10 µg/ml nGO-Cop-FA for 7h. a) HeLa cells, b) two-photon imaging of HeLa cells incubated for 6h with a 10 µg/ml nGO-Cop. Confocal imaging: Argon

laser Ex.488nm, Em.520-580nm. MP imaging: Ti:Sapphire (Mai Tai HP, Newport) femtosecond pulse laser Ex.960, Em.520-580nm.

The HeLa cells incubated with nGO-Cop (**Figure 5b**) for 6 h were excited at 960 nm and were detectable at 520-580 nm. The intracellular nGO were mainly localized in the cytoplasm and the signal-to-noise ratio was improved for PL detection. The PL from nGO was detectable both with argon ion laser (488nm) and the Ti:Sapphire femtosecond pulsed laser for two-photon excitation. Our data demonstrate that the copolymer-coated nGOs could be used as a bright optical probe for *in vitro* two-photon microscopy (**Figures 5 b**). An excitation with near-infrared wavelength has been shown to incur less scattering, photobleaching and photodamage in *in vivo* models and deep tissue imaging<sup>39,40</sup>. Two-photon microscopy excites the fluorophores in a femtoliter volume axially confined at the focal plane and the longer excitation wavelengths allow deeper penetration in the specimen in tissue samples<sup>41</sup>. Consequently, nGO are attractive choice for imaging probes for two-photon microscopy and exhibit detectable, bright PL in the visible range.

## 2.5. Effect of surface functionalization on cellular labelling

To facilitate cellular labelling, PEG-PEI copolymers were electrostatically adsorbed on the surface of the negatively charged nGO, as this mode of action proved to be efficient for cellular uptake of our nanodiamond-based composite structures in our previous study<sup>33</sup>. This resulted in a net positive charge (**Table 1**) induced by adsorption of highly positive charged PEI,<sup>42</sup> which prospectively improves the cellular uptake by interacting with negatively charged cell membranes, whereas the PEG part of copolymer provides colloidal stability by steric stabilization<sup>43</sup>.

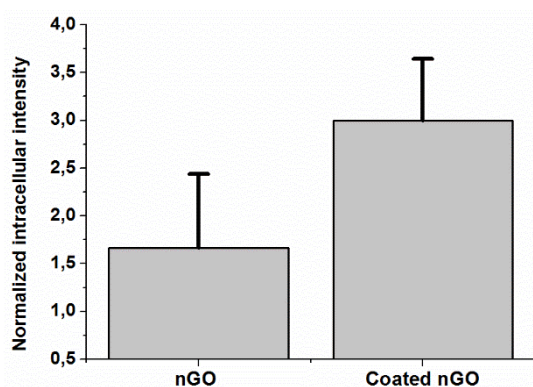


**Figure.6** Effect of surface coating (PEG-PEI copolymers, Cop) with affinity ligands (FA) improves cellular uptake and detectability in HeLa cells. HeLa cells were incubated with 10  $\mu\text{g}/\text{ml}$  of nGO and nGO-Cop-FA respectively for 24h. Both respective samples were imaged with confocal microscope using constant setting (Argon laser Ex.488nm, Em.528-630nm). The intracellular intensity due to particle uptake in the cells was measured and compared by ImageJ based intensity analysis. Error bars represent intensity variation among the individual sample.

Surface coating with PEG-PEI copolymers that had been additionally conjugated to the cancer-specific ligand FA was employed in order to maximize the affinity towards cancer cells, as FA is a generic targeting ligand for a variety of different cancers<sup>44,45,46</sup>. The intracellular intensity of nGO coated with FA-PEG-PEI copolymers (**Figure 7e**) was thereafter compared to that of cells incubated with pure nGO (**Figure 7b**) suggesting that the cellular uptake of nGO was enhanced by almost 100% by applying suitable organic modification, possibly also connected to better redispersibility of coated nanoparticles under aqueous conditions (**Table 1**) and especially so under complex biological conditions.

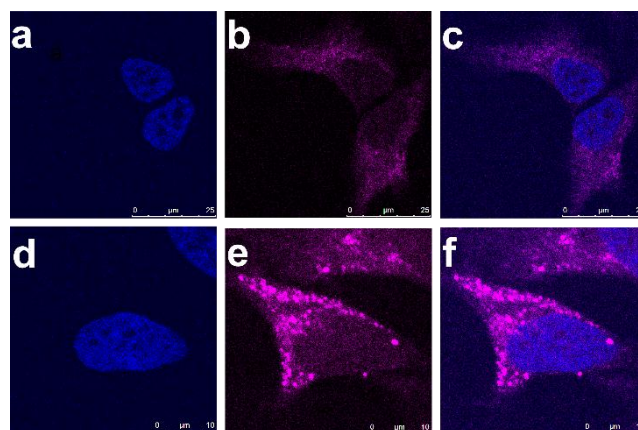


**Figure.7** a) Nuclei stained with Hoescht dye b) PL from pure nGO particles c) Overlay. The surface functionalization with copolymer improves uptake and quantum efficiency of nGO particles thus increases the detectability of cells. d) Hoescht nuclear dye e) enhanced cellular uptake can be seen in cells f) overlay images. Confocal imaging: Argon laser Ex.488nm, Em.528-630nm. MP imaging (Hoescht): Ti:Sapphire (Mai Tai HP, Newport) femtosecond pulse laser Ex.740, Em.blue wavelength range.

## 2.6. Excitation dependent emission

In tracking applications where several fluorescent reporters are employed, this usually compromises the need to be made between optimal sensitivity and spectral overlap of different labels. nGO has attractive photoluminescence properties because its excitation is dependent on emission, thus allowing emission in entire visible wavelength range<sup>47</sup>. To investigate if the multicolour emission property was retained also upon cellular labelling with the nGO, the nGO-Cop-FA incubated HeLa cells were fixed and imaged with different excitation wavelengths (Argon laser lines 458 nm, 488 nm, 514 nm and HeNe diode laser 633 nm) and they were collected in a narrow detection range to allocate real RGB colors (**Figure 8**).

Cite this: DOI: 10.1039/c0xx00000x

www.rsc.org/xxxxxx

ARTICLE TYPE

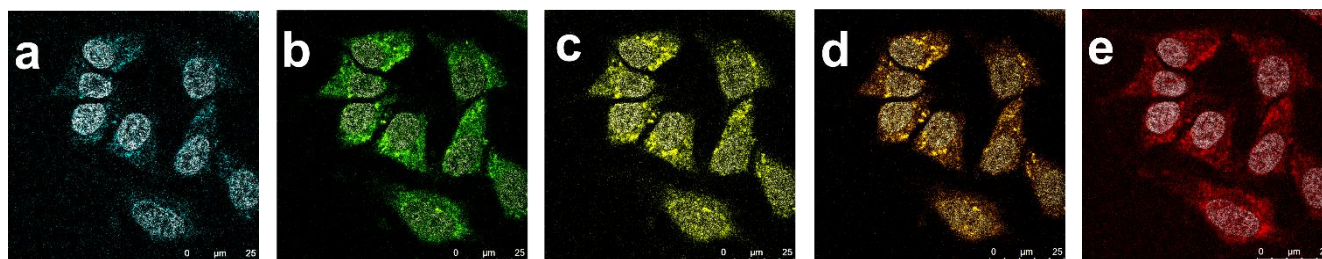


**Figure 8** a) Different argon laser excitation at 458 nm, 488 nm, 514 nm, 633 nm was used for nGO-Cop incubated cells. Emission from particles were collected at a) 470-500nm for excitation at 458nm, b) 528-558nm for excitation at 488nm, c) 558-588nm for excitation at 488nm, d) 584-618nm for excitation at 514nm and e) 649-703nm for excitation at 633nm. MP imaging (Hoescht): Ti:Sapphire (Mai Tai HP, Newport) femtosecond pulse laser Ex.740, Em. Blue wavelength range.

As can be seen in **Figure 8**, PL from nGO can be efficiently collected in a colour specific manner using a narrow bandwidth of wavelengths. nGO might thus offer great potential to use a combination of different fluorophores for imaging by using a constant nGO excitation and emission. This can be validated in **Figure 8**, where Hoechst nuclear stained cells were constantly excited by femtosecond MP laser, whereas nGO emission and excitation was varied. Therefore, unique emission properties of nGO allow it to be used with different existing cellular stains. nGO emission in the far red region is especially attractive to be exploited for *in vivo* imaging applications with different animal models<sup>48, 49</sup>. Application of the giant red-edge effect has thus far been non-existent, but the most obvious use of the phenomenon would be fluorescence wavelength tuning *in situ* by simply changing the excitation wavelength. This feature of nGO has now been presented in multiplexed *in vivo* imaging setup where optimal contrast can be tuned in relation to the other stains sample to provide the optimal contrast for each staining. Another practical use of nGOs in biological sensing as tuneable full spectrum fluorescent light sources, would be application of a single laser line to excite two labels with a single exposure, thus essentially doubling image acquisition speed and limiting the phototoxicity effects caused by excitation.

### 2.7. nGO distribution in daughter cells

Confocal imaging of dividing HeLa cells revealed that nGO was distributed evenly among the daughter cells (**Figure 9**). This further implies that nGO could be used for cellular detection for longer periods of times. Long term tracking or detection is important to address a range of quantitative cellular behaviours such as cell migration, cell division and apoptosis.

45

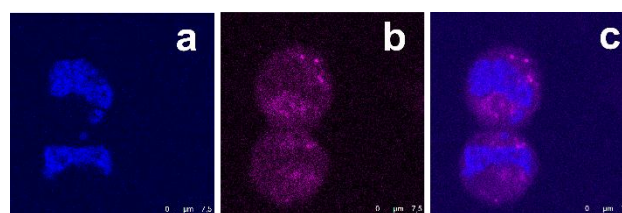


**Figure 9** Equivalent distribution of graphene oxide nanoparticle (nGO) among dividing daughter cells. Both the daughter cells contain nGO upon division. a) Hoechst stained nucleus, b) daughter cells carrying nGO and c) overlay.

50

Consequently, nGO acts a stable and non-toxic marker that remains localized in cells upon successive cell divisions. They can be detected in dividing cells and were detectable upon successive divisions till 1 week during the *in vivo* experiments (below). Cell labelling with nGO does not show any apparent effect on cellular functions such as division and proliferation. Therefore, nGO could be applied for long-term detection and tracking of primary cells in 3D *in vitro* cultures or in *in vivo* xenografts for events such as cancer cell metastasis<sup>50</sup>.

60

### 2.7. CAM model

The *ex ova* version of the CAM model was chosen to be a model for *in vivo* imaging. The *ex ova* model offers large surface area, easy access to microvasculature and implantation of nGO-Cop-FA labelled tumor cells<sup>22,51</sup>. Cancer cell lines (HeLa, intermediate FR; MDA-MB-231, high FR; and, A549 low FR) were incubated 24 h with the nGO-Cop-FA particles as cellular labels and implanted on the CAM on the 8th day. The model was allowed to continue to grow under clean and light restricted conditions (**Figure 10**).

70

40



**Figure.10** Shell-less (*ex ova*) egg in cell media containing weighing boats. Implantation of 10  $\mu\text{g/ml}$  nGO-Cop-FA labelled tumors over a highly vascularized CAM at day 8.

Vascularized tumors from HeLa, MDA-MB-231 and A549 cancer cell lines were successfully grown on CAM and intravascularization of implanted cancer cells was observed also adhesion to other foci on CAM.

30

## 2.8. Multiphoton *in vivo* imaging of nGO labeled tumors

To demonstrate nGO-Cop-FA's applicability in a preclinical setting, we recorded invasion of nGO-Cop-FA labelled tumors on both *in ova* and *ex ova* CAM models by two-photon imaging (**Figure 11**). nGO-Cop-FA-labelled HeLa, MDA-MB-231 and A549 cancer cells expressing folate receptors<sup>34</sup> were implanted over CAM and allowed to form tumors over an one week time period, whereafter they were imaged on a multiphoton microscope with excitation wavelength at 800 nm, and emission was detected at 430-480 nm. Employing two-photon imaging successfully circumvented the typical interference from autofluorescence of biological material at this wavelength range. The nGO-Cop-FA labelled cancer cells (**Figure 11 a-c**) were detectable with two-photon imaging after 1 week of tumor implantation. The CAM model thus provided technical simplicity, an *in vivo* environment and it was an especially suitable animal model for optical *in vivo* imaging in sub-cellular resolution. Imaging of nGO labelled tumors over CAM with multiphoton microscopy allowed deep tissue penetration, low amount of photodamage to the tumors and enhanced contrast for live imaging (**Figure 11 a-c**).

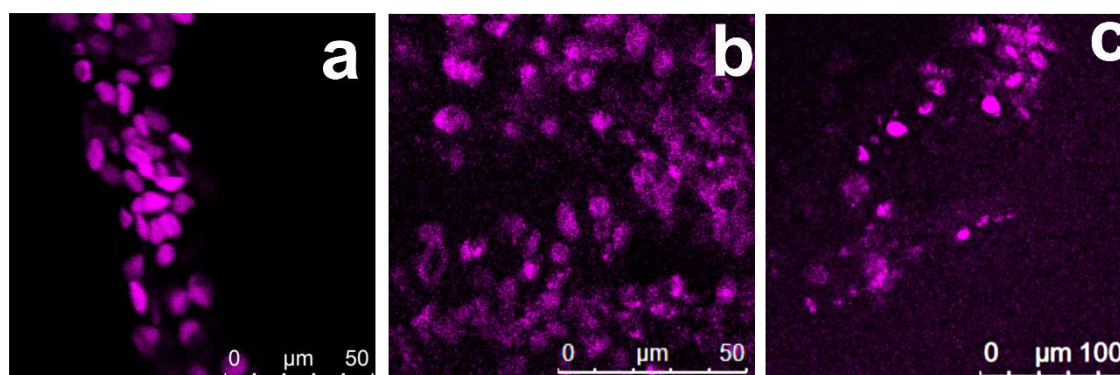


**Figure.11** Graphene oxide as an optical agent for *in vivo* imaging of tumors. Different cancer cells incubated with nGO-Cop-FA implanted on CAM for *in vivo* detection a) HeLa cells, b) A459 cells, c) MDA-MB-231 cells after one week of implantation, allowing tumors to form. [MP Ex. 800nm, Non descanned detector Em.430-480nm, 20X dip objective].

The cancer cell labelling with nGO-Cop-FA particles for 24 h incubation *in vitro* at a concentration of 10  $\mu\text{g/ml}$  was sufficient to detect them over CAM after the 8<sup>th</sup> day of implantation. The photoluminescence from the nGOs was strong enough image the circulating and arrested cancer cells in the dynamic environment of the live CAM model (**Supplementary Movie S7**). The cells remained viable as the non-toxic nature of nGO made them suitable for long term imaging even after 1 week of implantation, after which the chick development had to be terminated according to the standard CAM model procedure. The nGO-labelled implanted tumors were imaged a number of times over the 1 week period; by using low laser power we were able to avoid noticeable damage to the implanted cells/tumors or blood vessels of the live embryo. In the field of personalized oncology there is a growing need for cellular staining that would have minimal impact on tumor biology and could be applied on primary cells to be examined in 3D cultures and *in vivo* xenografts. These results demonstrate the potential of nGO as optical probe for non-invasive *in vivo* imaging.

## 55 Conclusion

In this work, we have comprehensively studied a novel type of nGO to realize its potential for biomedical applications. We have successfully coated the nGO nanoparticles with organic copolymers, with or without the cancer-specific affinity ligand folic acid, to increase the biomedical applicability of nGO with special focus on cellular labelling for *in vivo* cancer imaging using a very optically transparent and ethical animal model, the CAM model. The organic coating was shown to enhance the performance of nGO in a biological setting in a number of ways: improved dispersability under aqueous conditions, increased quantum yield as well as enhanced cellular labelling efficiency in cancer cells with improved cellular detectability as a result. The PL properties of nGO were characterized using laser spectrometry in a standard confocal setup and in non-linear two-photon microscopy that is an especially facilitative biomedical imaging technique for *in vivo* imaging. The spectra were measured in a physiological environment and in a standard

LSCM-setup to demonstrate the wide applicability of nGO as nano-sized labels. The nGO, functionalized or not, were shown to be safe during *in vitro* studies and as a material assured biocompatibility for *in vivo* detection of cancer cells. The nGOs were readily taken up due to their small size, they can be labelled over a single passage, they distribute evenly between daughter cells and are non-toxic so they can be labelled in quantities sufficient to monitor the tumor growth over several weeks. In conclusion, we have explored and demonstrated their applicability in tracking of cell populations in an *in vivo* model to establish them as biocompatible, non-invasive and photostable optical labels with broad versatility that can be utilized in conjunction with any other label due to their wide and tuneable PL emission properties.

## Acknowledgements

The authors would like to acknowledge LSK Poultry Oy, 23800 Laitila, Finland, Dr. Shishir Jaikishan, Prof. J. Peter Slotte, Helena Saarento, Jari Korhonen, Senthil Kumar Rajendran, Markus Peurla and Laboratory of Electron Microscopy, University of Turku, Finland. The financial contribution from Academy of Finland projects #137101 (NP, EvH, JMR) #140193 & 278812 (JMR) #260599 (NP, EvH, DSK, VM, JMR) #126998 (T.N. and P.H.), #15-29-01290 (TD, SB and IV) from RFBR (Russian Foundation for Basic Research) and the Doctoral Education Network in Materials Research at Åbo Akademi University (NP) are gratefully acknowledged.

## Notes and references

<sup>a</sup> Pharmaceutical Sciences Laboratory, Faculty of Science and Engineering, Åbo Akademi University, 20520 Turku, Finland

<sup>b</sup> E-mail: [jerosenh@abo.fi](mailto:jerosenh@abo.fi)

<sup>c</sup> Laboratory of Biophysics, Faculty of Medicine, University of Turku, FI-20520 Turku, Finland

<sup>d</sup> E-mail: [tuonar@utu.fi](mailto:tuonar@utu.fi)

<sup>e</sup> Laboratory of Physical Chemistry, Faculty of Science and Engineering, Åbo Akademi University, 20500 Turku, Finland

<sup>f</sup> Department of Physics, Lomonosov Moscow State University, 119991 Moscow, Russia

<sup>g</sup> Section for Haematology, Clinical Institute 2, University of Bergen, 5020 Bergen, Norway

<sup>h</sup> General Physics Institute, Russian Academy of Sciences, 119991 Moscow, Russia

<sup>i</sup> National Research Nuclear University MEPhI, Moscow 115409, Russia

<sup>j</sup> International Technology Center, Raleigh, North Carolina, United States.

<sup>k</sup> † Electronic Supplementary Information (ESI) available. See DOI: 10.1039/b000000x/

- 1 S. C. Ray, A. Saha, N. R. Jana and R. Sarkar, *J. Phys. Chem. C*, 2009, **113**, 18546–18551.
- 2 S. Chandra, P. Das, S. Bag, D. Laha and P. Pramanik, *Nanoscale*, 2011, **3**, 1533.
- 3 P. Juzenas, A. Kleinauskas, P. G. Luo and Y.-P. Sun, *Appl. Phys. Lett.*, 2013, **103**, 063701.
- 4 T. S. Hauck, R. E. Anderson, H. C. Fischer, S. Newbigging and W. C. W. Chan, *Small*, 2010, **6**, 138–144.
- 5 S. N. Baker and G. A. Baker, *Angew. Chem. Int. Ed.*, 2010, **49**, 6726–6744.
- 6 S.-T. Yang, X. Wang, H. Wang, F. Lu, P. G. Luo, L. Cao, M. J. Meziani, J.-H. Liu, Y. Liu, M. Chen, Y. Huang and Y.-P. Sun, *J. Phys. Chem. C*, 2009, **113**, 18110–18114.

- 7 J.-H. Liu, S.-T. Yang, X.-X. Chen and H. Wang, *Curr. Drug Metab.*, 2012, **13**, 1046–1056.
- 8 L. Cao, M. J. Meziani, S. Sahu and Y.-P. Sun, *Acc. Chem. Res.*, 2013, **46**, 171–180.
- 9 X. Zhang, S. Wang, C. Zhu, M. Liu, Y. Ji, L. Feng, L. Tao and Y. Wei, *J. Colloid Interface Sci.*, 2013, **397**, 39–44.
- 10 S. Zhu, S. Tang, J. Zhang and B. Yang, *Chem. Commun.*, 2012, **48**, 4527–4539.
- 11 X. Sun, Z. Liu, K. Welscher, J. T. Robinson, A. Goodwin, S. Zaric and H. Dai, *Nano Res.*, 2008, **1**, 203–212.
- 12 G. Eda, Y.-Y. Lin, C. Mattevi, H. Yamaguchi, H.-A. Chen, I.-S. Chen, C.-W. Chen and M. Chhowalla, *Adv. Mater.*, 2010, **22**, 505–509.
- 13 J. Shen, Y. Zhu, C. Chen, X. Yang and C. Li, *Chem. Commun.*, 2011, **47**, 2580–2582.
- 14 C. Galande, A. D. Mohite, A. V. Naumov, W. Gao, L. Ci, A. Ajayan, H. Gao, A. Srivastava, R. B. Weisman and P. M. Ajayan, *Sci. Rep.*, 2011, **1**.
- 15 S. C. Hens, G. Cunningham, G. McGuire and O. Shenderova, *Nanosci. Nanotechnol. Lett.*, 2011, **3**, 75–82.
- 16 S. Ciftan Hens, W. G. Lawrence, A. S. Kumbhar and O. Shenderova, *J. Phys. Chem. C*, 2012, **116**, 20015–20022.
- 17 J. Peng, W. Gao, B. K. Gupta, Z. Liu, R. Romero-Aburto, L. Ge, L. Song, L. B. Alemany, X. Zhan, G. Gao, S. A. Vithayathil, B. A. Kaipparattu, A. A. Marti, T. Hayashi, J.-J. Zhu and P. M. Ajayan, *Nano Lett.*, 2012, **12**, 844–849.
- 18 J. M. Rosenholm, A. Meinander, E. Peuhu, R. Niemi, J. E. Eriksson, C. Sahlgren and M. Lindén, *ACS Nano*, 2009, **3**, 197–206.
- 19 D. Şen Karaman, T. Gulín-Sarfraz, G. Hedström, A. Duchanoy, P. Eklund and J. M. Rosenholm, *J. Colloid Interface Sci.*, 2014, **418**, 300–310.
- 20 J. Azzarello, M. A. Ilnat, B. P. Kropp, L. A. Warne and H.-K. Lin, *Biomed. Mater.*, 2007, **2**, 55.
- 21 X. Liu, X. Wang, A. Horii, X. Wang, L. Qiao, S. Zhang and F.-Z. Cui, *Nanoscale*, 2012, **4**, 2720–2727.
- 22 E. I. Deryugina and J. P. Quigley, *Histochem. Cell Biol.*, 2008, **130**, 1119–1130.
- 23 A. Chwalibog, E. Sawosz, S. Jaworski, M. Kutwin, A. Hotowy, M. Wierzbicki, M. Grodzik, N. Kurantowicz, B. Strojny and L. Lipinska, *Int. J. Nanomedicine*, 2014, 3913.
- 24 R. Auerbach, R. Lewis, B. Shinnars, L. Kubai and N. Akhtar, *Clin. Chem.*, 2003, **49**, 32–40.
- 25 R. Auerbach, L. Kubai, D. Knighton and J. Folkman, *Dev. Biol.*, 1974, **41**, 391–394.
- 26 A. Garcia-Bennett, M. Nees and B. Fadeel, *Biochem. Pharmacol.*, 2011, **81**, 976–984.
- 27 R. Gref, A. Domb, P. Quelled, T. Blunk, R. H. Müller, J. M. Verbavatz and R. Langer, *Adv. Drug Deliv. Rev.*, 1995, **16**, 215–233.
- 28 O. Boussif, F. Lezoualc'h, M. A. Zanta, M. D. Mergny, D. Scherman, B. Demeneix and J. P. Behr, *Proc. Natl. Acad. Sci.*, 1995, **92**, 7297–7301.
- 29 L. Bergman, J. Rosenholm, A.-B. Öst, A. Duchanoy, P. Kankaanpää, J. Heino and M. Lindén, *J. Nanomater.*, 2008, **2008**, 51:1–51:9.
- 30 T. A. Dolenko, S. A. Burikov, J. M. Rosenholm, O. A. Shenderova and I. I. Vlasov, *J. Phys. Chem. C*, 2012, **116**, 24314–24319.
- 31 J. Wei, J. Qiu, L. Ren, K. Zhang, S. Wang and B. Weeks, *Sci. Adv. Mater.*, 2014, **6**, 1052–1059.
- 32 Q. Mei, K. Zhang, G. Guan, B. Liu, S. Wang and Z. Zhang, *Chem. Commun.*, 2010, **46**, 7319–7321.
- 33 N. Prabhakar, T. Näreoja, E. von Haartman, D. Ş. Karaman, H. Jiang, S. Koho, T. A. Dolenko, P. E. Hänninen, D. I. Vlasov, V. G. Ralchenko, S. Hosomi, I. I. Vlasov, C. Sahlgren and J. M. Rosenholm, *Nanoscale*, 2013, **5**, 3713–3722.
- 34 R. Senthilkumar, D. Ş. Karaman, P. Paul, E. M. Björk, M. Odén, J. E. Eriksson and J. M. Rosenholm, *Biomater. Sci.*, 2014.
- 35 R. Meier, T. D. Henning, S. Boddington, S. Tavri, S. Arora, G. Piontek, M. Rudelius, C. Corot and H. E. Daldrop-Link, *Radiology*, 2010, **255**, 527–535.
- 36 M. García-Díaz, S. Nonell, A. Villanueva, J. C. Stockert, M. Cañete, A. Casadó, M. Mora and M. L. Sagristá, *Biochim. Biophys. Acta*, 2011, **1808**, 1063–1071.

- 37 T.-G. Iversen, T. Skotland and K. Sandvig, *Nano Today*, 2011, **6**, 176–185.
- 38 L. Feng, X. Yang, X. Shi, X. Tan, R. Peng, J. Wang and Z. Liu, *Small Weinh. Bergstr. Ger.*, 2013, **9**, 1989–1997.
- 5 39 F. Helmchen and W. Denk, *Nat. Methods*, 2005, **2**, 932–940.
- 40 K. Svoboda and S. M. Block, *Annu. Rev. Biophys. Biomol. Struct.*, 1994, **23**, 247–285.
- 41 M. Rubart, *Circ. Res.*, 2004, **95**, 1154–1166.
- 42 T. Xia, M. Kovochich, M. Liang, H. Meng, S. Kabehie, S. George, J. I. Zink and A. E. Nel, *ACS Nano*, 2009, **3**, 3273–3286.
- 10 43 R. A. Sperling and W. J. Parak, *Philos. Trans. R. Soc. Math. Phys. Eng. Sci.*, 2010, **368**, 1333–1383.
- 44 A. R. Hilgenbrink and P. S. Low, *J. Pharm. Sci.*, 2005, **94**, 2135–2146.
- 15 45 C. M. Paulos, J. A. Reddy, C. P. Leamon, M. J. Turk and P. S. Low, *Mol. Pharmacol.*, 2004, **66**, 1406–1414.
- 46 S. A. Kularatne and P. S. Low, *Methods Mol. Biol. Clifton NJ*, 2010, **624**, 249–265.
- 47 N. Puvvada, B. N. P. Kumar, S. Konar, H. Kalita, M. Mandal and A. Pathak, *Sci. Technol. Adv. Mater.*, 2012, **13**, 045008.
- 20 48 B. W. Rice, M. D. Cable and M. B. Nelson, *J. Biomed. Opt.*, 2001, **6**, 432–440.
- 49 S. Tanaka and S. Kizaka-Kondoh, *Gan To Kagaku Ryoho*, 2008, **35**, 1272–1276.
- 25 50 E. B. Voura, J. K. Jaiswal, H. Mattoussi and S. M. Simon, *Nat. Med.*, 2004, **10**, 993–998.
- 51 N. A. Lokman, A. S. F. Elder, C. Ricciardelli and M. K. Oehler, *Int. J. Mol. Sci.*, 2012, **13**, 9959–9970.

30